




## Article

# Film Properties of Heparin Cross-Linked with Epichlorohydrin in Absence or Presence of Imidazole

Ivan Šimkovic <sup>1,\*</sup>, Filip Gučmann <sup>2</sup>, Michal Hricovíni <sup>1</sup>, Raniero Mendichi <sup>3</sup>, Edmund Dobročka <sup>2</sup>, Alberto Giacometti Schieron <sup>4</sup>, Daniele Piovani <sup>4</sup>, Stefania Zappia <sup>4</sup> and Miloš Hricovíni <sup>1</sup>

<sup>1</sup> Institute of Chemistry, Slovak Academy of Sciences, 84538 Bratislava, Slovakia; chemmike@savba.sk (M.H.); chemilos@savba.sk (M.H.)

<sup>2</sup> Institute of Electrical Engineering, Slovak Academy of Sciences, Dúbravská Cesta 9, 84104 Bratislava, Slovakia; filip.gucmann@savba.sk (F.G.); edmund.dobrocka@savba.sk (E.D.)

<sup>3</sup> Problem Solving, Innovation Support Complex Polymeric and Elastomeric Materials Analysis, Molecular and Rheological Characterization Complex Polymers Via Roma 7, 20067 Milan, Italy; rmendichi@libero.it

<sup>4</sup> Istituto di Scienze e Tecnologie Chimiche “G. Natta”, Via A. Corti 12, 20133 Milan, Italy; alberto.giacometti@scitec.cnr.it (A.G.S.); daniele.piovani@scitec.cnr.it (D.P.); stefania.zappia@scitec.cnr.it (S.Z.)

\* Correspondence: chemsimk@savba.sk

**Abstract:** We cross-linked unfractionated heparin (H) using epichlorohydrin (E), in the absence or presence of imidazole (I), using various ratios of H, E, and I substances. The objectives and goals were to use the reaction for the preparation of medical materials suitable for blood sample applications. Nuclear magnetic resonance indicated the involvement of an H-end sequence [H-(1→4)-β-D-GlcA-(1→3)-β-D-Gal-(1→3)-β-D-Gal-(1→4)-β-D-Xyl-α-Ser] in the linkage with the 2-hydroxypropyl bridge. The yields of the individual experiments were found to increase in the following ratios: 1H/1E/3I (24%) < 1H/1E/2I (32%) < 1H/3E (42%) < 1H/1E/1I (46%) < 1H/2E (64%) < 1H/1E (77%). According to size-exclusion chromatography with multiple-angle light scattering (SEC-MALS) analysis, the mass at the peak increased in the following order: H (9292 g/mol) < 1H/1E (9294 g/mol) < 1H/2E (9326 g/mol) < 1H/3E (9708 g/mol) < 1H/1E/2I (11,212 g/mol) < 1H/1E/3I (12,301 g/mol) < 1H/1E/1I (13,800 g/mol) and in the reverse order with the increase in amount of epichlorohydrin and imidazole, i.e., 1H/1E > 1H/2E > 1H/3E and 1H/1E/1I > 1H/1E/2I > 1H/1E/3I. X-ray diffraction revealed that all prepared films were amorphous. An evaluation of the surface morphology using atomic force microscopy (AFM) confirmed a relatively low films roughness (~0.9–3.6 nm). The surface reduced elastic modulus, determined by the PeakForce quantitative nanomechanical mapping (PF-QNM) technique, was found to increase by up to ~63% for films cross-linked with E in the absence of I when compared with the results for the H substrate. A negligible change in modulus was, however, observed for films cross-linked in the presence of I, or was even reduced by ~15% (1H/1E/3I) compared to that for the H substrate. This could be explained by the parallel cross-linking of H only with E within its serine end unit and in competition with only one nitrogen of I. According to the highest yield (77%) of 1H/1E, the preferred product is the following: H-(1→4)-β-D-GlcA-(1→3)-β-D-Gal-(1→3)-β-D-Gal-(1→4)-β-D-Xyl-α-Ser-CH<sub>2</sub>-CH(OH)-CH<sub>2</sub>-OH. For the 1H/1E/1I (46% yield), 1H/1E/2I (32%), and 1H/1E/3I (24%) products, the cross-linked motif was the same, and the difference represented the surplus amount of the imidazolium cation ionically bound to the heparin anionic groups.

**Keywords:** heparin; cross-linking; epichlorohydrin; imidazole; film properties; medical applications



**Citation:** Šimkovic, I.; Gučmann, F.; Hricovíni, M.; Mendichi, R.; Dobročka, E.; Schieron, A.G.; Piovani, D.; Zappia, S.; Hricovíni, M. Film Properties of Heparin Cross-Linked with Epichlorohydrin in Absence or Presence of Imidazole. *Polysaccharides* **2024**, *5*, 715–730. <https://doi.org/10.3390/polysaccharides5040045>

Academic Editor: Martin Gericke

Received: 28 August 2024

Revised: 14 October 2024

Accepted: 5 November 2024

Published: 10 November 2024



**Copyright:** © 2024 by the authors. Licensee MDPI, Basel, Switzerland. This article is an open access article distributed under the terms and conditions of the Creative Commons Attribution (CC BY) license (<https://creativecommons.org/licenses/by/4.0/>).

## 1. Introduction

Heparinized nanocomposites are expected to represent a new category of materials for medical applications [1]. However, the use of these materials is currently not widespread. For example, only intravascular catheters are covered with heparin films. Selective modification of heparin represents a first step in the preparation of environmentally

safe heparinized all-polysaccharide composites, with components soluble and insoluble in water, to replace environmentally undesirable plastic materials [2]. Heparin (H) is a structurally rather complex polysaccharide, which is composed of repeating disaccharide units comprising a uronate (either  $\beta$ -D-glucuronate (GlcA) or  $\alpha$ -L-iduronate (IdoA) and a hexosamine, 2-amino-2-deoxy  $\alpha$ -D-glucose ( $\alpha$ -D-glucosamine; GlcN) units. The repeating disaccharide can be substituted by O- and N-sulphate groups (denoted here with S) at positions 2-O- of the uronate and 6-O- (or more rarely, position 3-O-) of the glucosamine residue. Furthermore, the glucosamine unit is predominantly N-sulphated, so the predominant heparin residues consist of GlcNS<sub>6S</sub> and IdoA<sub>2S</sub> units. Thus, H is highly substituted with ion exchanging groups, which makes it soluble in water, even after modification with amine or the trimethylammonium-2-hydroxypropyl spacer [3,4]. The use of epichlorohydrin (E) for H cross-linking to prepare hydrogels was not previously studied [5], although the cross-linking of bagasse with E in the presence of imidazole, or hyaluronic acid cross-linking with E, was reported earlier [6,7]. Using E for cross-linking does not pose any significant health hazard or cancer threat, as the cross-linked product does not contain an epoxy ring. This is because of the high reactivity of E that ensures that it fully forms 2-hydroxypropyl bridges or is degraded by water to form glycerol. The epichlorohydrin chemistry is highly active in paper-related industries, and technological development is necessary to prevent health harm for the operators of such processes. The cross-linking of polysaccharides with imidazole (I) derivatives or with other quaternary groups is a known method for the fractionation and solubilization of agricultural by-products [8,9]. According to previously reported nuclear magnetic resonance (NMR) results, the known end sequence on the unfractionated heparin end is: H-(1→4)- $\beta$ -D-GlcA-(1→3)- $\beta$ -D-Gal-(1→3)- $\beta$ -D-Gal-(1→4)- $\beta$ -D-Xyl- $\alpha$ -Ser [10]. Heparin and heparan sulfate represent the most diverse family of glycosaminoglycans (GAGs), and for this reason, their exploitation in the field of macromolecular chemistry is rather difficult [11,12]. However, we hypothesize that the above-mentioned H-end sequence is the region where the cross-linking could take place. These products might find their use in, e.g., dialysis where they would help to overcome the involvement of plastic components [13]. Another important application where heparin films can bring about environmentally friendly innovation is in blood collection tubes for diagnostic methodologies related to blood analysis [1].

The cross-linking of polysaccharides with E usually takes place under alkaline or acidic conditions. However, for H, these conditions are too drastic and could cause its degradation [14]. For this reason, we have chosen to run the reaction in deionized water (DW) at room temperature (RT) and at a molar ratio of H/E/H<sub>2</sub>O = 1:1:1000. The advantage is that the reaction could take place in a solution under homogeneous conditions and the cross-linked product is still soluble in water due to the presence of both carboxyl and sulfate groups, which are simultaneously inert to the E attack. The epoxy group in E reacts preferentially with the amine serine end group rather than with the sterically hindered free hydroxyl groups of H. In this way, the H-(1→4)- $\beta$ -D-GlcA-(1→3)- $\beta$ -D-Gal-(1→3)- $\beta$ -D-Gal-(1→4)- $\beta$ -D-Xyl- $\alpha$ -Ser-CH<sub>2</sub>-CH(OH)-CH<sub>2</sub>-OH derivative could be formed.

Another component which could affect the reactivity of epichlorohydrin is imidazole, which is used in ionic liquid technologies [15]. In the presence of I, the situation is different due to the presence of two nitrogen atoms on its ring, which requires a different cross-linking mechanism. It involves one E molecules reacting first with imidazole and subsequently, with the heparin serine end group. Our objectives are to identify the optimal reaction conditions and to obtain a product with a minimal content of monofunctional modification with E. We have experimented with three H/E ratios (1/1, 1/2, and 1/3), as well as with three H/E/I ratios (1/1/1, 1/1/2, and 1/1/3). Our aim in this study is to find a simple and reproducible approach for the preparation of well-characterized H derivatives under environmentally safe conditions, with an acceptable yield and molecular weight of the products, and which are higher than those of H.

The prepared cross-linked H-based samples were characterized by nuclear magnetic resonance (NMR) and size-exclusion chromatography with multiple-angle light scattering (SEC-MALS) analysis in a water solution, and the prepared films were studied by the X-ray diffraction (XRD), atomic force microscopy (AFM), and PeakForce quantitative nanomechanical mapping (PF-QNM) technique. We observed that the cross-linking of H increases the molecular weight of the prepared derivatives and results in improved mechanical surface properties of the prepared films.

## 2. Materials and Methods

### 2.1. Materials

Heparin (H) Merck, H4874-1G, Source SLCC 4685, sodium salt from porcine intestinal mucosa; C, 20.92; H, 2.89; N, 1.93; S, 10.29;  $M_p = 9292$  g/mol;  $M_w = 11,065$  g/mol; molecular mass by weight ( $M_w$ )/molecular mass by number ( $M_n$ ) = 1.51; recovered mass: 93.5%; imidazole (ACROS ORGANICS, Belgium, 301872500-250G); ( $\pm$ )-epichlorohydrin, 99% (Aldrich, Cat.: E105-5); and all other chemicals were used without further purification.

### 2.2. Cross-Linking of H with E

H (0.5730 g, IdoA<sub>2S</sub>-Glc<sub>NS,6S</sub>, 1 mM) was dissolved in deionized water (DW; 18 mL), and E was added (0.0782 mL, 1 mM). The mixture was stirred (1000 rpm) at RT for 24 h. The reaction was stopped by diluting the mixture with DW (pH = 7.15) and dialyzed (3.5 kDa MWCO dialysis tubing, Union Carbide, Houston, TX, USA; pH = 5.85). After lyophilization, a heparin derivate was produced (1H/1E; 0.5100 g), and a 77% yield was obtained. The yield was determined as  $\{[\text{weight of product}/(\text{weight of substrate} + \text{weight of E used})] \times 100\} = 0.51/0.573$  g of H + 0.0925 g of E; C, 21.52; H, 3.16; N, 1.98; S, 10.46;  $M_p = 9294$  g/mol;  $M_w = 11,948$  g/mol;  $M_w/M_n = 1.91$ ; SEC-MALS recovered mass: 98.1%.

At H/E = 1/2 molar ratio and under identical conditions to those used above, the pH changed from 7.70 to 5.9 after dialysis, and by lyophilization, 1H/2E was obtained (0.4871 g; 64% yield [0.4871 g of product/0.573 g of H + 0.1850 g of E]; C, 21.85; H, 3.02; N, 2.03; S, 10.55;  $M_p = 9326$  g/mol;  $M_w = 12,509$  g/mol;  $M_w/M_n = 2.11$ ; SEC-MALS recovered mass: 98.3%).

At H/E = 1/3 molar ratio and under identical conditions to those used above, the pH changed from 7.40 after dialysis to 6.18 and by lyophilization 1H/3E was obtained (0.3610 g, 42% yield [0.3610 g of product/0.573 g of H + 0.2775 g of E]; C, 21.72; H, 3.13; N, 2.07; S, 10.70;  $M_p = 9708$  g/mol;  $M_w = 14,234$  g/mol;  $M_w/M_n = 1.90$ ; SEC-MALS recovered mass: 99.0%).

### 2.3. Cross-Linking of H with E in the Presence of I

H (0.5730 g, IdoA<sub>2S</sub>-Glc<sub>NS,6S</sub>, 1 mM) was dissolved in DW (18 mL), mixed with I (0.0681 g, 1 mM) and E (0.0782 mL, 1 mM) was added; the mixture was then processed under the identical conditions as those used above at pH = 8.35, before dialysis, and 5.63, before lyophilization (1H/1E/1I, 0.6246 g, 46% yield [0.6246 g of product/0.573 g of H + 0.0925 g of E + 0.681 g of I]; C, 28.51; H, 3.94; N, 5.12; S, 9.04;  $M_p = 11,212$  g/mol;  $M_w = 20,317$  g/mol;  $M_w/M_n = 1.80$ ; SEC-MALS recovered mass: 38.5%).

Additional experiments were carried out at H/E/I = 1/1/2, at pH = 8.36, after stopping the reaction, and pH = 5.77, after dialysis before lyophilization (1H/1E/2I, 0.6647 g, 32% yield [0.6647 g of product/0.573 g of H + 0.0925 g of E + 1.363 g of I]; C, 31.11; H, 4.23; N, 6.95; S, 8.50;  $M_p = 11,212$  g/mol;  $M_w = 12,755$  g/mol;  $M_w/M_n = 1.62$ ; recovered mass: 90.5%).

At an H/E/I = 1/1/3 ratio, the experiment was carried out as above, with a pH = 8.29, after stopping the reaction and before the dialysis, and a pH = 5.48 before lyophilization; (0.6418 g, 24% yield [0.6418 g of product/0.573 g of H + 0.0925 g of E + 2.043 g of I]; C, 30.88; H, 4.15; N, 7.08; S, 8.66;  $M_p = 12,301$  g/mol;  $M_w = 13,218$  g/mol;  $M_w/M_n = 1.34$ ; recovered mass: 88.2%).

#### 2.4. Analytical Methods

High-resolution NMR measurements were performed on all samples (~20 mg/0.75 mL D<sub>2</sub>O (ARMAR Cat. No 014400.0010; 99.96%)) at 25 °C on a Bruker 600 MHz spectrometer equipped with a 5 mm cryogenic probe. <sup>1</sup>H and <sup>13</sup>C chemical shifts were referenced to the heparin acetyl group (2.05 ppm/24.75 ppm). The pH-in-D<sub>2</sub>O (pD) values of the solutions were determined using 20 mg samples, according to the Nguyen and Rabenstein method [16]. The rest of the experimental conditions were identical to those previously described [4,7].

The elemental compositions were determined using a FLASH 2000 organic elemental analyzer (Thermo Fisher Scientific; furnace temperature: 950 °C; PTFE column, 6 mm o. d./5 mm inner diameter × 2 m; 65 °C; helium was used as a carrier and reference gas, flow: 140 and 100 mL/min, respectively; oxygen flow: 250 mL/min; 720 s run time; 12 s sampling delay; 5 s injection end).

The characterization of the molecular weight distribution (MWD) was performed using a multi-angle laser light scattering (MALS) absolute detector connected on-line to a size-exclusion chromatographic (SEC or GPC) system. A differential refractometer (DRI) was used as online concentration detector. An aqueous SEC mobile phase (0.1M CH<sub>3</sub>COONH<sub>4</sub> at pH = 7.0) and two TSKgel PW columns (4000-3000, with pore sizes of 17 and 12 μm) from Tosoh Bioscience (D) were used. The SEC-MALS experimental conditions were as follows: 35 °C temperature; 0.8 mL/min flow rate; 150 μL injection volume; about 10 mg/mL sample concentration. The calibration constant of the MALS detector was calculated using toluene as a standard, assuming a Rayleigh factor of  $1.406 \times 10^{-5} \text{ cm}^{-1}$ . The angular normalization of the MALS detector was performed using a concentrated solution of BSA globular protein (M = 66.4 kg/mol, R<sub>g</sub> = 2.9 nm), assumed to act as an isotropic scatterer. The specific refractive index increment, with respect to the solvent (dn/dc) of H (dn/dc = 0.132 mL/g), was measured offline using a Chromatix KMX-16 differential refractometer. The difference in the dn/dc values of the derivatives with respect to native H was lower than the uncertainty of the experimental measurement; therefore, an identical dn/dc value was also used for the derivatives. The sample “recovered mass”, expressed as % of the injected mass, refers to the sample mass eluting (i.e., recovered) from the SEC columns. The recovered mass is calculated from the area of the signal of the concentration detector (differential refractometer) after accurate calibration. Details of the other analytical methods used were described previously [4,7].

Similarly, to the methods used in our previous work [17], the X-ray diffraction measurements were performed using a Bruker D8 DISCOVER diffractometer, equipped with an X-ray source with a rotating Cu anode operating with a lamp exhibiting 12 kW power, 40 kV voltage, and 300 mA current. Parallel beam geometry, with a parabolic Goebel mirror in the primary beam, was used; the beam divergence was ~0.03°. To suppress the influence of surface roughness and other irregularities and to avoid the change of size, shape, and X-ray penetration depth into the sample during the measurement, a grazing incidence (GI) setup, with constant angle of incidence  $\alpha = 2^\circ$ , was used. Measurements were performed in an angular range of 15°–40°, with a 0.05° step size and a 1 s integration time per step.

A Bruker MultiMode 8-HR AFM, using Si Bruker RTESPA-525 probes (spring constant  $K \sim 200 \text{ N/m}$ ; <https://www.brukerafmprobes.com/p-3915-rtespa-525.aspx>, accessed on 27 August 2024) in PeakForce tapping mode in air and under room temperature, was used to study the surface morphology and nanomechanical surface properties of all prepared polysaccharide films. The following method was used for all samples: 0.01 g of the sample was dissolved in 1 mL of deionized water (DW), transferred to a Petri dish (5.5 cm in diameter), and dried in the refrigerator at 5 °C until it reached a constant weight. The surface morphology and spatially-resolved mechanical properties were evaluated from several different measured locations (3–5) to decrease the uncertainty and improve the reliability of the extracted values. A constant force setpoint (~60–90 nN) was maintained during each measurement to avoid undesired variations in indentation depth, which would otherwise influence the extracted values. The mechanical properties of prepared films

were determined using the PF-QNM technique. First, all RTESPA 525 probes used were calibrated for cantilever deflection sensitivity, spring constant, and tip radius for the used indentation depth. Cantilever deflection sensitivity was measured on an incompressible substrate (with respect to the cantilever stiffness), i.e., sapphire.

The determined deflection sensitivities for the cantilevers used for the measurement were in the range  $41.1 \pm 0.4$  nm/V– $71.1 \pm 0.4$  nm/V; the cantilever spring constants, determined using the Sader method [18], were in the range  $154 \pm 10$  N/m– $201 \pm 13$  N/m. The average indentation depth was determined for each measured sample at corresponding force set-point using measured force curves and was typically on the order of several nanometers. The tip radius at the corresponding indentation depth was determined using the tip reconstruction and qualification function of the Bruker Nanoscope Analysis software (version 1.90), assuming a tip radius determined from the topographical evaluation of the Ti roughness test sample RS-12M, supplied by Bruker.

The retraction parts of the measured force curves at each pixel of the scanned area were evaluated using the Derjaguin–Muller–Toporov (DMT) model [19,20], implemented in Nanoscope Analysis software (Bruker), to obtain quantitative information regarding the surface reduced elastic modulus ( $E^*$ ). To avoid ambiguity, and due to the unknown values of the Poisson's ratio ( $\nu$ ) of our samples, we present values of the reduced elastic modulus instead of the true elastic modulus ( $E$ ). Assuming a much higher elastic modulus of the used AFM tip than that of the sample ( $E_s$ ), the reduced elastic modulus is defined as  $E^* = E_s / (1 - \nu_s^2)$ , where  $\nu_s$  is the Poisson's ratio of the sample.

### 3. Results and Discussion

#### 3.1. Cross-Linking

In the experiments in absence of I, where H was cross-linked with E at 1/1, 1/2, and 1/3 molar ratios, the respective obtained yields were 77%, 64%, and 42%. These results indicate that all the H-serine end groups were already fully involved in the reaction at 1/1 of the H/E ratio. This indicates that these conditions were optimal for the 1H/1E ratio to react with the serine-end group to produce the sequence: H-(1→4)-β-D-GlcA-(1→3)-β-D-Gal-(1→3)-β-D-Gal-(1→4)-β-D-Xyl-α-Ser-CH<sub>2</sub>-CH(OH)-CH<sub>2</sub>-OH, with the highest observed yield. At the ratio of 1H/2E, we expect that the product with the obtained 64% yield was likely: H-(1→4)-β-D-GlcA-(1→3)-β-D-Gal-(1→3)-β-D-Gal-(1→4)-β-D-Xyl-α-Ser-CH<sub>2</sub>-CH(OH)-CH<sub>2</sub>-O-CH<sub>2</sub>-CH(OH)-CH<sub>2</sub>-OH. Analogously, the 1H/3E ratio could produce the third 2-hydroxypropyl on the serine-end unit: H-(1→4)-β-D-GlcA-(1→3)-β-D-Gal-(1→3)-β-D-Gal-(1→4)-β-D-Xyl-α-Ser-CH<sub>2</sub>-CH(OH)-CH<sub>2</sub>-O-CH<sub>2</sub>-CH(OH)-CH<sub>2</sub>-O-CH<sub>2</sub>-CH(OH)-CH<sub>2</sub>-O-CH<sub>2</sub>-CH(OH)-CH<sub>2</sub>-OH, which led to the obtained 42% yield.

In the presence of I, when the amount of I was increased at a constant amount of H and E, i.e., at H/E/I ratios of 1/1/1, 1/1/2, and 1/1/3, the obtained yields were 46%, 32%, and 24%. The imidazole content in all products was also confirmed by elemental analysis, indicating an increased nitrogen content (see Section 2). Since at the H/E/I ratio of 1/1/1, the yield was the highest, we assume that one I molecule is taking part in the reaction with the heparin serine-end unit to form a new sequence (46% yield), as shown in Figure 1. At the ratio of H/E/I = 1/1/2 (32% yield), the sequence might be formed as shown in Figure 2.

At the H/E/I ratio of 1/1/3, the remaining imidazolium cation could be attached to some sterically available uronate anion, which led to the lowest yield (24%).

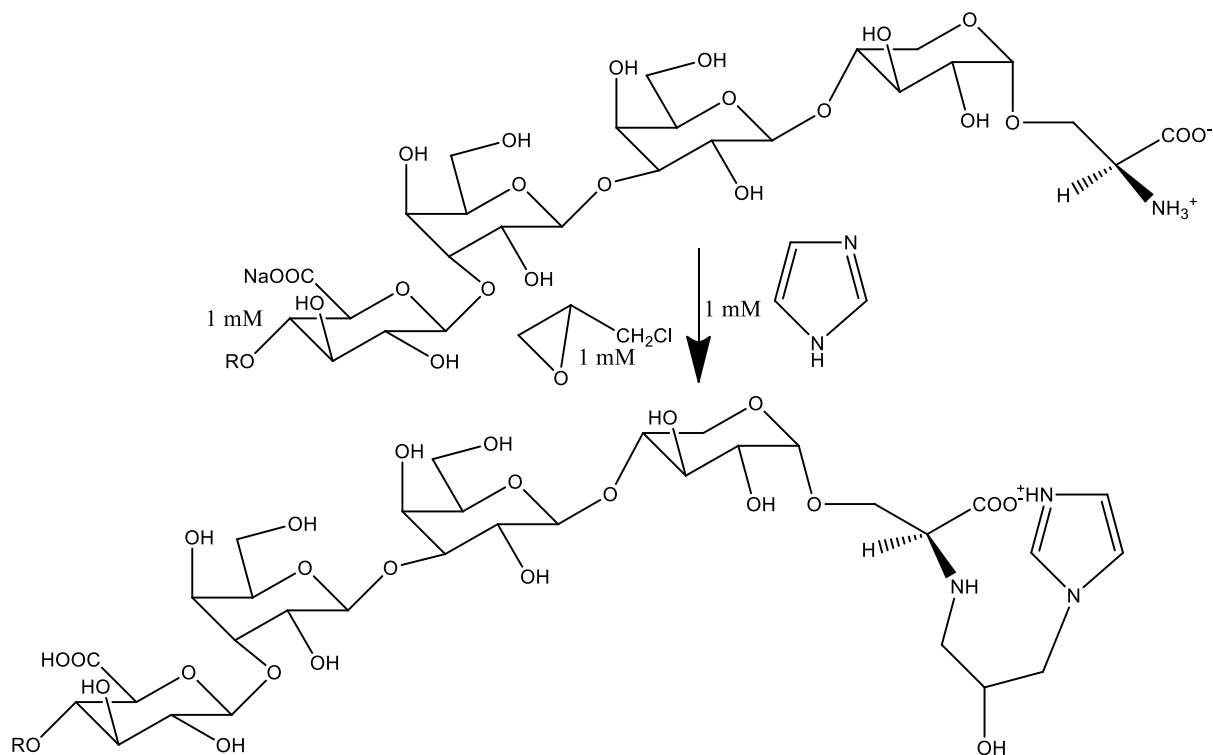


**Figure 1.** The proposed reaction at H/E/I ratio of 1:1:1.

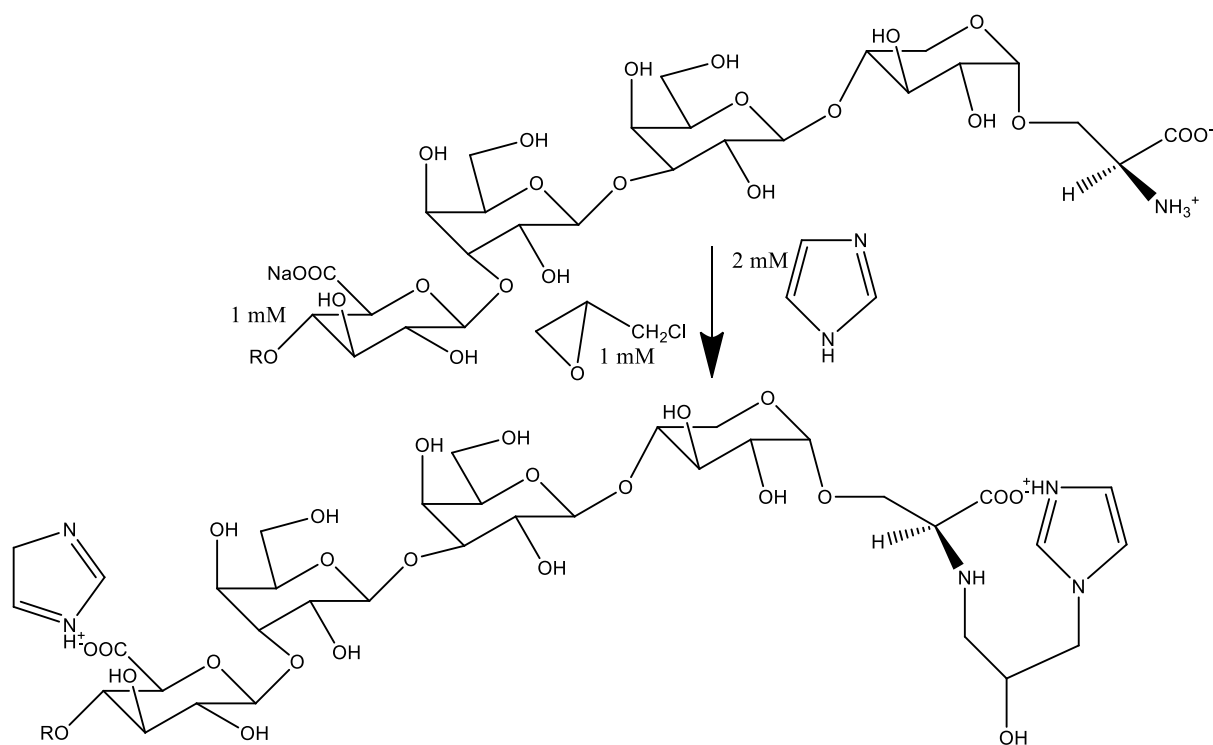


**Figure 2.** The proposed reaction at the H/E/I ratio of 1:1:2.

### 3.2. NMR Analysis

In comparison to  $^1\text{H}$  NMR spectrum of the unfractionated H, based on our previous studies on H [4], the 2D NMR analysis method is more informative for the identification of new substituents and it prevents overlapping of the signals. Ten anomeric signals were detected in the HSQC spectrum of H (Figure 3). This result is also in agree-

ment with the known data [18]. The signals at 5.42/99.26 ppm (Glc<sub>NS,6S</sub>-Ido<sub>2S</sub>) and 5.22/102.08 ppm (Ido<sub>2S</sub>-Glc<sub>NS,6S</sub>) were the most intense, similar to previous observations and specifications used by Mauri et al. for unfractionated H [10]. The signals at 5.58/100.30 ppm (Glc<sub>N,6S</sub>-GlcA), 5.57/98.92 ppm (Glc<sub>NS,3S,6S</sub>), 5.04/104.73 ppm (Ido<sub>2S</sub>-Glc<sub>NS,6S</sub>), 4.98/104.57 ppm (IdoA-Glc<sub>NS</sub>), 4.66/106.72 ppm (GalA + Gal), 4.54/104.40 ppm (GlcA-Glc<sub>N6,3S,6S</sub>), 4.50/105.23 ppm (GlcA-Glc<sub>NAc</sub>), and 4.47/105.73 ppm (Xyl-Ser) ppm are minor signals, with the Xyl linked to serine with an  $\alpha$ -glycosidic bond at the end of the heparin chain [10]. The 6 Glc<sub>NS,6S</sub>-Ido<sub>2S</sub> signal occurs at 4.28, 4.42/68.97 ppm, and the signals of non-sulfated 6 GlcA-Glc<sub>NS,3S,6S</sub> are observed at 3.84, 3.88/62.42 ppm [10]. Additionally, minor CH<sub>2</sub> signals of the 5 Xyl unit occur at 3.41, 4.12/65.83 ppm. The COSY spectrum (not shown here) showed that the signal at 3.92/56.61 ppm belongs to 2 Glc<sub>NAc</sub>, the signal at 3.78/85.48 ppm is due to 2 GlcA + Gal, and that of the 3 GlcA + Gal units is at 3.84/84.98 ppm [10]. The above assignments confirmed the presence of the H-end motif: H-(1 $\rightarrow$ 4)- $\alpha$ -D-GlcNS6S-(1 $\rightarrow$ 4)- $\beta$ -D-GlcA-(1 $\rightarrow$ 4)- $\beta$ -D-Gal-(1 $\rightarrow$ 3)- $\beta$ -D-Gal-(1 $\rightarrow$ 3)- $\beta$ -D-Xyl- $\alpha$ -Ser [10,21].

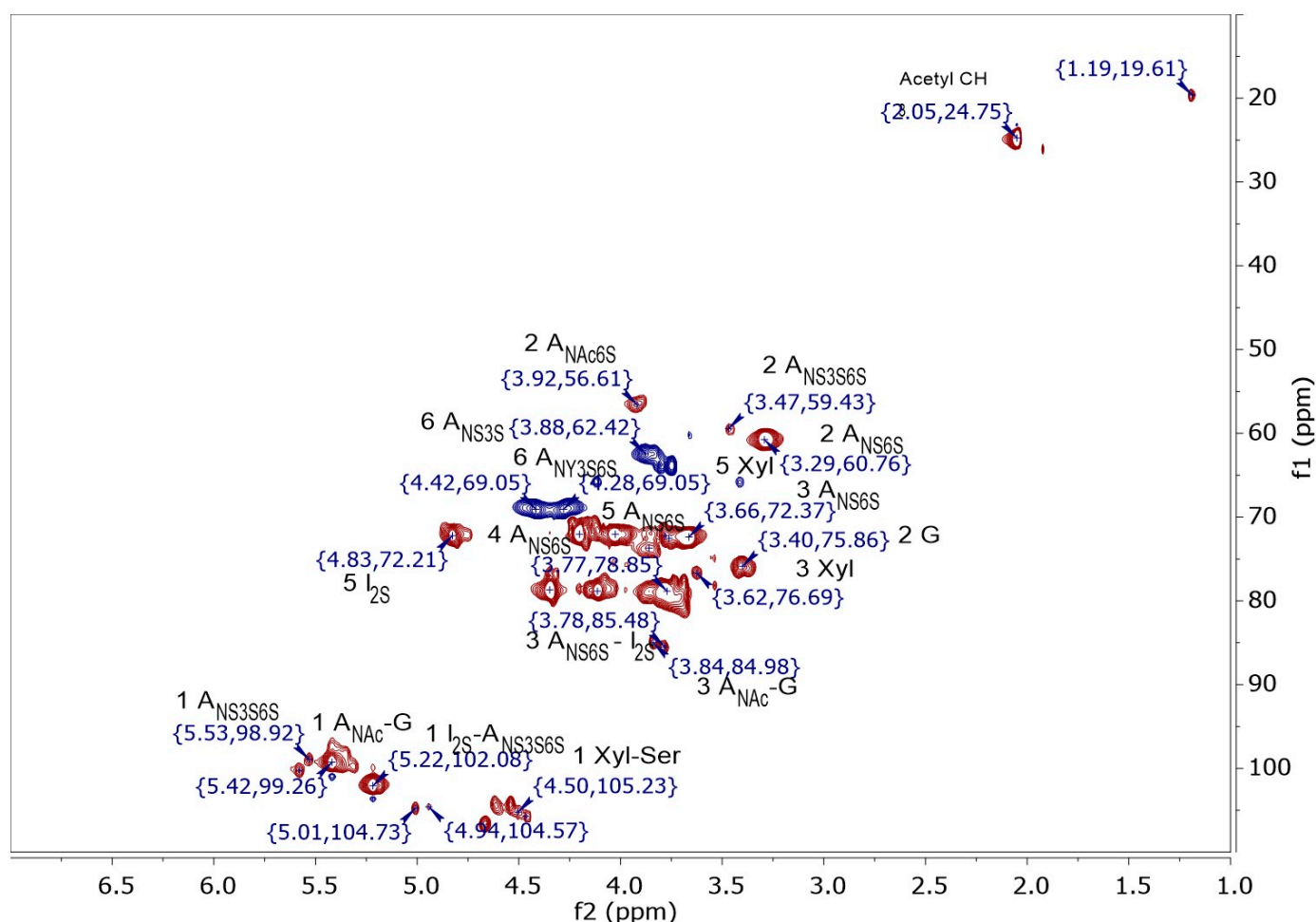


**Figure 3.** HSQC spectrum of unfractionated H (the C-H groups are in red and CH<sub>2</sub> groups in blue).

The number of anomeric signals is identical for heparin cross-linked with epichlorohydrin at a 1/1 molar ratio at the highest yield (1H/1E; 77% yield) in the HSQC spectrum (Figure 4) as to that for reference H. The signals at 5.42/100.59 ppm (Glc<sub>NS,6S</sub>-Ido<sub>2S</sub>) and 5.27/102.06 ppm (Ido<sub>2S</sub>-Glc<sub>NS,6S</sub>) were the most intense. The presence of the A<sub>NS,3S,6S</sub> (5.54/99.20 ppm) and GlcA-Glc<sub>NS,6S</sub> signals (4.63/104.52 ppm) indicates that the GlcA units linked to A<sub>NS,6S</sub> were not degraded. The 2 Glc<sub>NS,6S</sub>-GlcA signal occurs at 3.41/75.67 ppm and 3 Glc<sub>NS,6S</sub>-GlcA at 3.40/75.70 ppm. New signals at 3.73, 3.79/48.21 ppm (-CH<sub>2</sub>-), 3.46/56.81 ppm, 3.47/59.45 ppm, and 4.06/57.11 ppm [-CH(OH)],

related to the 2-hydroxypropyl cross-linking bridge ( $-\text{CH}_2-\text{CH}(\text{OH})-\text{CH}_2-$ ), were observed. The rest of the ring signals were identical to those for the H sample. The hydroxypropyl bridge linking serine,  $\text{H}-(1\rightarrow4)-\beta\text{-D-GlcA}-(1\rightarrow3)-\beta\text{-D-Gal}-(1\rightarrow3)-\beta\text{-D-Gal}-(1\rightarrow4)-\beta\text{-D-Xyl}-\alpha\text{-Ser}-\text{CH}_2-\text{CH}(\text{OH})-\text{CH}_2-\text{OH}$ , is supported by  $-\text{CH}(\text{OH})-$  signals at 2.92/47.47 ppm, 3.93/56.49 ppm, and 3.46/59.48 ppm in the HSQC spectrum. These three signals might represent central parts of three different mono-functionally linked 2-hydroxypropyl groups. The shape of the bridge is also supported by the fact that there are no interactions between the  $-\text{CH}(\text{OH})-$  groups at 2.92/47.47, 3.93/56.46, and 3.46/59.48 ppm and any other signal in the corresponding HMBC spectrum of the 1H/1E sample.

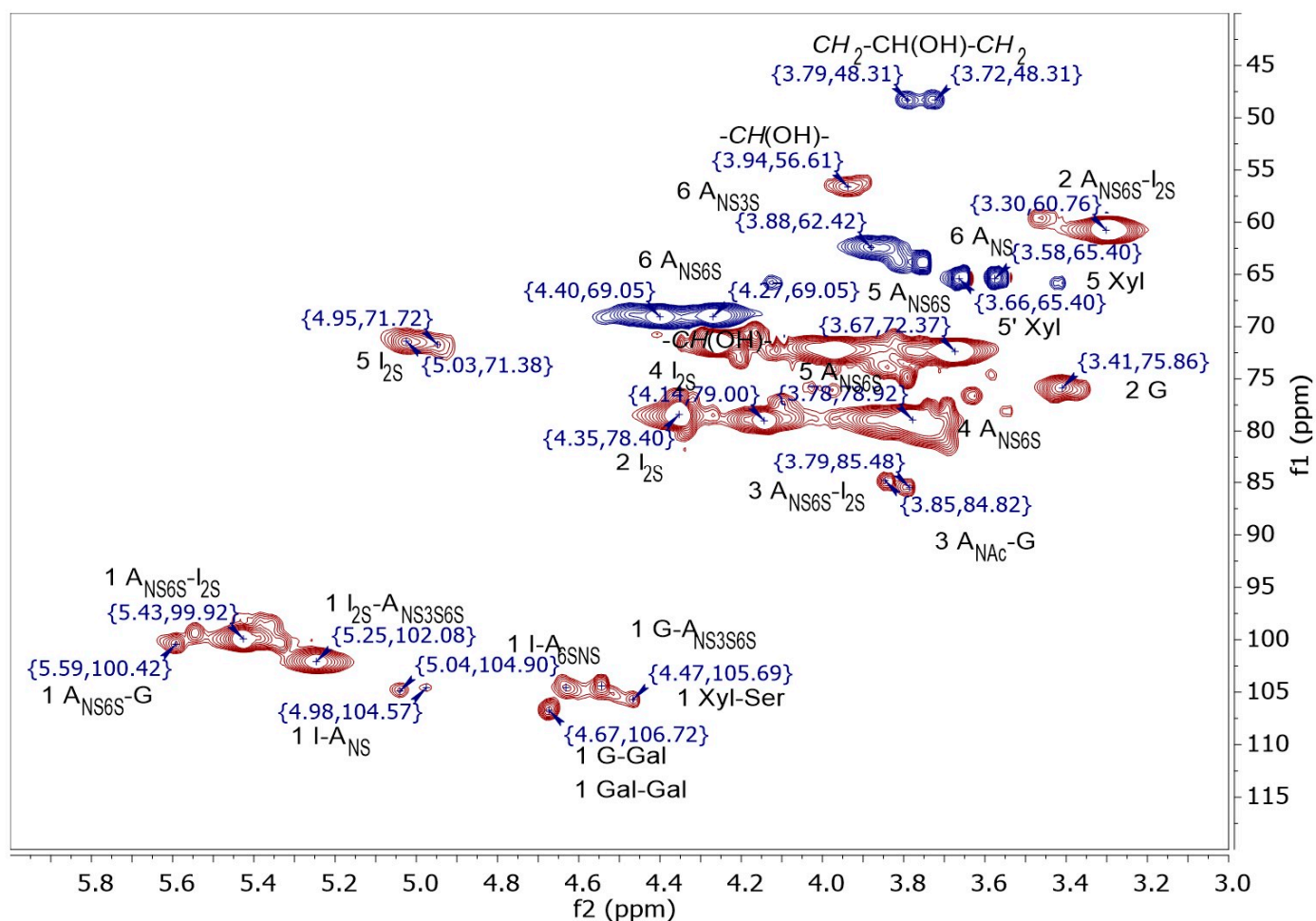


**Figure 4.** HSQC spectrum of 1H/1E (the red signals are related to C-H and the blue to  $\text{CH}_2$  groups).

When cross-linked at a 1/2 ratio (1H/2E), the yield slightly decreased (64%). The NMR data for 1H/2E were identical to those for 1H/1E. The cross-linking at a 1/3 ratio (1H/3E) decreased the yield even further down to 42%. The HSQC data were also identical to those for 1H/1E.

The HSQC spectrum of the 1H/1E/1I sample (Figure 5) also revealed ten anomeric signals ( $\text{pD} = 7.40$ ; 46% yield). The second-highest yield was observed for 1H/1E/2I ( $\text{pD} = 5.97$ ; 32%). The anomeric signals were assigned analogously to 1H/1E/1I, i.e., [5.35/100.00 ppm ( $\text{Glc}_{\text{NS},6\text{S}}\text{-IdoA}_{2\text{S}}$ ), 5.44/99.60 ppm ( $\text{GlcA}_{\text{NAc}}$ ), 5.24/99.54 ppm ( $\text{Glc}_{\text{NAc}}\text{-GlcA}$ ), 5.33/98.38 ppm ( $\text{Glc}_{\text{NS}}\text{-IdoA}$ ), 5.57/98.74 ppm ( $\text{Glc}_{\text{NS},6\text{S}}$ ), 5.48/99.40 ppm ( $\text{Glc}_{\text{NS}}\text{-GlcA}$ ), 5.56/100.48 ppm ( $\text{Glc}_{\text{NS},6\text{S}}\text{-GlcA}$ ), 5.14/102.01 ppm ( $\text{IdoA}_{2\text{S}}\text{-Glc}_{\text{NS},6\text{S}}$ ), 5.01/104.78 ppm ( $\text{IdoA-Glc}_{6\text{S}}$ ), 4.55/104.19 ppm ( $\text{IdoA-Glc}_{\text{NS}}$ ), 4.67/106.73 ppm ( $\text{Glc} + \text{Gal}$ ), 4.61/104.80 ppm ( $\text{GalA-Glc}_{\text{NS},6\text{S}}$ ), 4.62/103.80 ppm ( $\text{GlcA-Glc}_{\text{NS}}$ ), 4.53/105.30 ppm ( $\text{GlcA-Glc}_{\text{NAc}}$ ), and 4.47/105.72 ppm (Xyl-Ser)]. Additionally, two new  $-\text{CH}_2-$  groups, at 3.66/65.19 and 3.76/63.61 ppm, and four new  $-\text{CH}(\text{OH})-$  groups, at 2.92/47.42, 3.90/56.39, 3.37/59.54,



and 4.59/65.89 ppm, were observed. The first two CH(OH) groups (2.92/47.42 and 3.93/56.49 ppm) were also present in the 1H/1E experiment, while the other two -CH<sub>2</sub>- (3.66/65.19 ppm and 3.76/63.61 ppm) and CH(OH) groups observed at 3.37/59.59 ppm and 4.59/65.89 ppm are new, and we assume that they are related to the imidazolium rings.

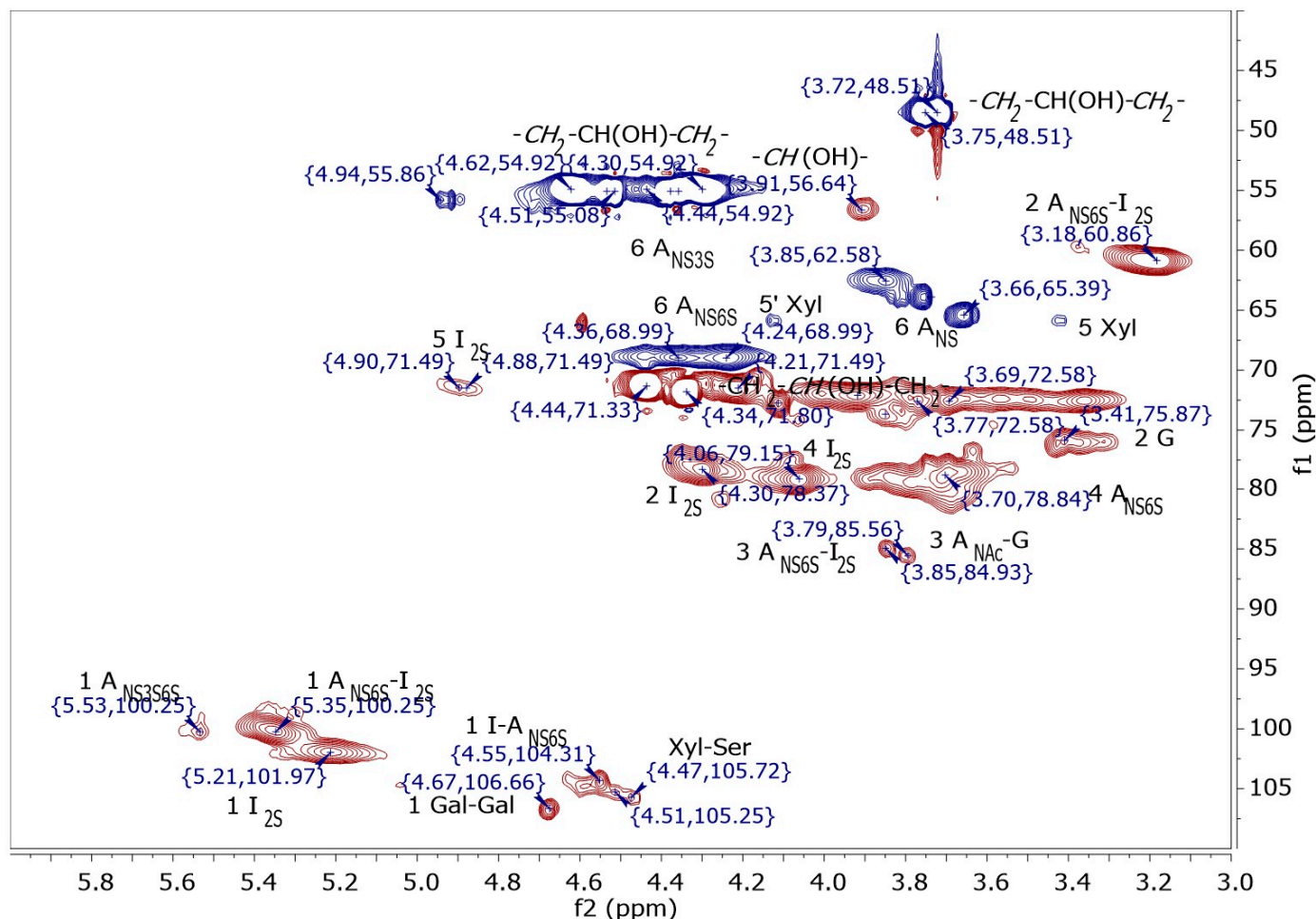


**Figure 5.** HSQC spectrum of the 1H/1E/1I sample (the red signals are related to C-H and the blue to CH<sub>2</sub> groups).

### 3.3. SEC-MALS Analysis

Figure 6 shows the SEC-MALS profiles of all the investigated samples. The molar mass of H substrate ( $M_w = 11,065$  g/mol) was the lowest of all the samples, with  $M_p = 9292$  g/mol and polydispersity at  $M_w/M_n = 1.51$ . The 1H/1E sample showed following values:  $M_p = 9294$  g/mol;  $M_w = 12,509$  g/mol and  $M_w/M_n = 1.91$ . The further increase in the determined values ( $M_p = 9326$  g/mol;  $M_w = 12,509$  g/mol and  $M_w/M_n = 2.11$ ) was observed for the 1H/2E sample and the 1H/3E sample ( $M_p = 9708$  g/mol;  $M_w = 14,234$  g/mol;  $M_w/M_n = 1.90$ ). The increase in  $M_p$  continued further for samples 1H/1E/2I (11,212 g/mol) < 1H/1E/3I (12,301 g/mol) < 1H/1E/1I (13,800 g/mol), while for  $M_w$ , the order was different: 1H/1E/2I (12,755 g/mol) < 1H/1E/3I (13,218 g/mol) < 1H/1E/1I (20,317 g/mol). The solubility of the samples exhibited the following increasing order: 1H/1E/1I (38.5%) < 1H/1E/3I (88.2%) < 1H/1E/2I (90.5%) < H (93.5%) < 1H/1E (98.1%) < 1H/2E (98.3%) < 1H/3E (99.0%), determined by the recovered mass of the SEC-MALS experiments. Unfortunately, the gyration radius values could not be determined due to the low molecular weights of the prepared samples.

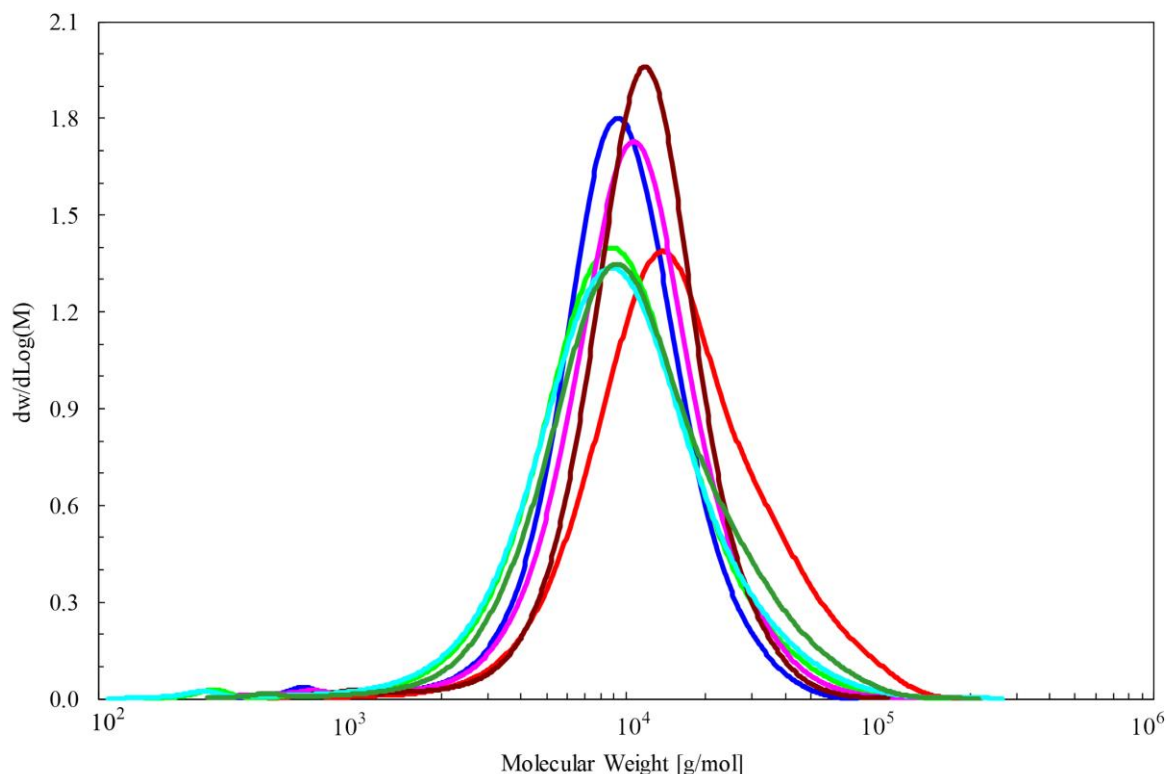


**Figure 6.** Comparison of SEC-MALS profiles of H (dark blue), 1H/1E (light green), 1H/2E (cyan), 1H/3E (dark green), 1H/1E/2I (violet), 1H/1E/3I (brown), and 1H/1E/1I (red) samples.

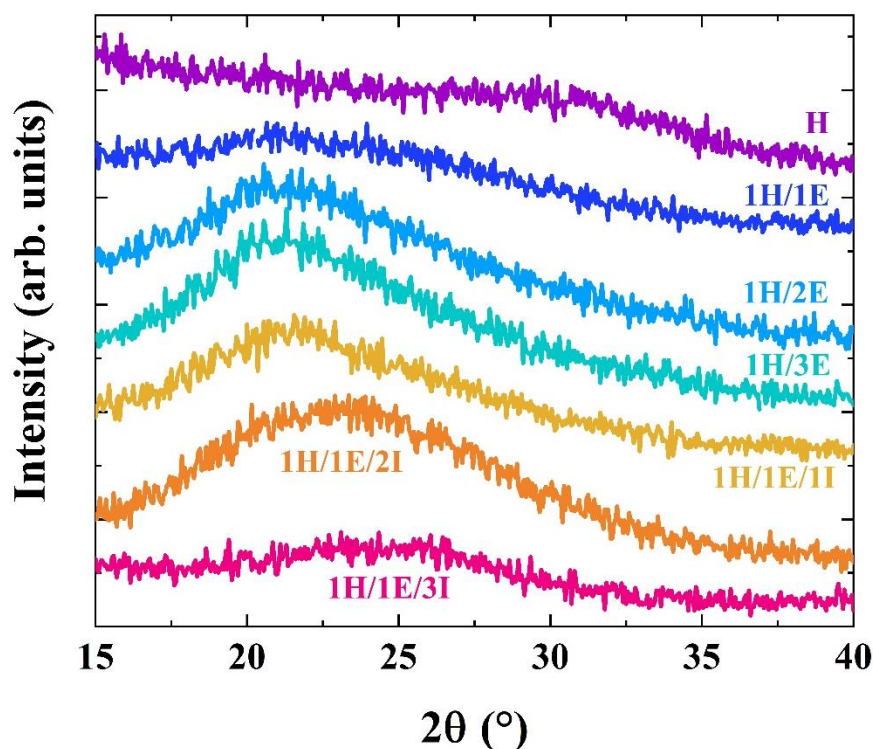
### 3.4. XRD Analysis of Films

Figure 7 shows the XRD scans of the prepared films. Reference H and all of the cross-linked macromolecules were amorphous, supporting our conclusion that the modification did not take place on the main H chain. While a weak reflection was observed at a  $\sim 20\text{--}22^\circ$  angle for the cross-linked products with certain amount of E (1H/1E, 1H/2E, 1H/3E, 1H/1E/1I), the remaining two I-containing products (1H/1E/2I and 1H/1E/3I) did not show this feature in the measured diffractogram. This could indicate that the cross-linking process used might have supported the development of a certain symmetry of the first four products and an asymmetry for the remaining two products. Similar XRD signals at a  $\sim 22^\circ$   $2\theta$  angle were previously attributed to low-molecular-weight heparin fractions, which were able to form nanoparticles of  $\sim 200$  nm size [22]. As will be discussed subsequently, the surface morphology of several prepared fractions showed varying degrees of surface particles of similar size ( $\sim 150\text{--}250$  nm), and therefore, we suspect that the  $20\text{--}22^\circ$   $2\theta$  reflection observed here may be partially related to these. No other crystalline structures related to heparin derivatives are known [23,24]. Typically, minor crystalline structures are related to residual components of the prepared film supra-structure, not chemically bonded to heparin.

### 3.5. AFM and PF-QNM Analysis

Figure 8a–g shows the measured surface morphology of all prepared heparin-based films, represented by  $2 \times 2 \mu\text{m}^2$  scans. Representative corresponding line profiles are also shown. The box and whisker plot in Figure 8h shows the statistical distribution of the root-mean-square (RMS) surface roughness extracted from several  $2 \times 2 \mu\text{m}^2$  scans acquired at various locations across the surface of the measured films. The evaluation of surface roughness reflects the upper surface of the film after the liquid derivatives were poured into the Petri dishes and dehydrated. Potentially different viscosities of the prepared derivatives may have resulted in slightly different thicknesses of the prepared films; however, we do not expect this to have any significant effect on the resulting determined surface roughness,

which was more significantly affected by various particles and pores present on the film surfaces. While no clear trend regarding roughness was observed related to the cross-linking with E and I, the reference heparin showed the widest spread of roughness values, which can be attributed to the large number of pores, ~15–100 nm deep across the surface of the H layer, and also to the presence of various particles (~150–250 nm). Similar pores were only observed in the 1H/3E film; however, they occurred less frequently. Films 1H/2E and 1H/1E/2I showed the lowest surface roughness (~1 nm), which was related to the much-decreased number of spherical particles, which were otherwise present in all the remaining films. The following increasing trend of average surface roughness was observed: 1H/2E (0.9 nm) < 1H/1E/2I (1.0 nm) < 1H/1E (2.1 nm) < 1H/1E/1I (2.2 nm) < 1H/3E (2.3 nm) < H (3.5 nm) < 1H/1E/3I (3.6 nm). This indicates that the most cross-linked films exhibit a decreased roughness of the surfaces when compared to those of H. The best result was observed in the 1H/2E sample, which indicates the optimum result for dimer hydroxypropyl, formed on the serine end-unit. The experiments containing, I exhibit higher roughness values with increasing amounts of I.



**Figure 7.** Symmetric XRD scans of prepared films.

The observed surface morphologies of the prepared H-based films showed similarities to those of some of the previously studied seaweed carrageenan films; however, those generally exhibited a higher surface roughness (~2.4–18.6 nm) for scans of similar dimensions [23]. Some similarities, such as the size of granular features, were also observed in the line profiles. This behavior may be explained by the high density of the strongly charged carboxyl and sulfate groups with relatively low molecular weight ( $M_w = 11,065$  g/mol;  $M_w/M_n = 1.54$ ) present in the H film in comparison to those of the carrageenans in the films prepared from seaweed extracts. The values at the peak ( $M_p$ ) were considerably larger for the carrageenans (from 77.8 to 994.0 kg/mol) [23]. Although the  $M_w$  value of the 1H/1E sample increased only slightly (19,900 g/mol;  $M_w/M_n = 1.54$ ) compared to that for the seaweed polysaccharides, their surface roughness values were significantly different (i.e., higher for the seaweed-based films). The lowest average RMS surface roughness of ~1 nm for the 1H/2E and 1H/1E/2I films was even lower than the results obtained for the seaweed polysaccharides [14]. The further increase in molecular weight observed for the

1H/1E/1I sample ( $M_w = 24,200$  g/mol;  $M_w/M_n = 1.56$ ) resulted in a slight increase in the average RMS surface roughness value of  $\sim 2.2$  nm. All the above surface roughness values are comparable with the values determined for the chitosan/heparin multilayer films [25], as well as with the RMS values determined on gold covered with PEI cross-linked heparin covered with synthetic polymers used for antidote heparin [24].

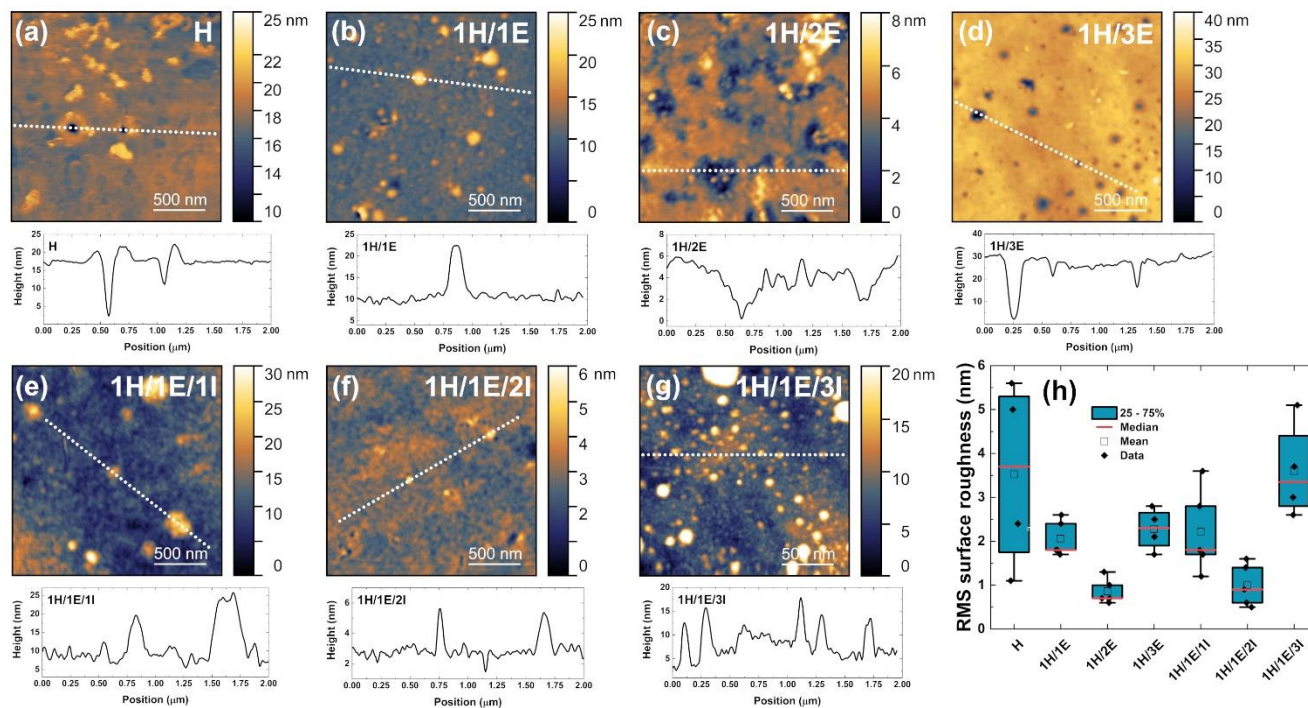


**Figure 8.** Surface morphology and corresponding representative line profiles (taken along the white dotted lines) of (a) H, (b) 1H/1E, (c) 1H/2E, (d) 1H/3E, (e) 1H/1E/1I, (f) 1H/1E/2I, and (g) 1H/1E/3I samples determined by the AFM; (h) statistical distributions of RMS surface roughness for all films.

Currently, only a limited number of reports dedicated to the evaluation of the mechanical properties of heparin films [4,22,23], or other polysaccharides [24–26], exist. To evaluate the influence of E and I cross-linking on heparin’s mechanical properties, the PeakForce quantitative nanomechanical mapping technique was applied to all prepared films, and the reduced DMT elastic modulus was determined. We note that this technique is limited to probing only the surface or near-surface mechanical properties of the films, and these may differ significantly from those of the bulk, where other mechanical phenomena may play an additional role. Nevertheless, the surface mechanical properties could be important to evaluate, e.g., the wear resistance and longevity of the prepared films in various applications.

The spatially resolved maps of the reduced elastic modulus ( $E^*$ ) of all the prepared films are shown in Figure 9a–g. These maps represent the same measurement locations as those shown in the surface morphology scans Figure 8a–g. The box and whisker plot in Figure 9h shows a statistical distribution of the  $E^*$  values extracted from the scans in Figure 8a–g, assuming their normal distribution, and are representative for several measurement locations. Here, the green-colored boxes represent the data falling within the lower (Q1) and upper (Q3) quartiles of a probability density function accounting for 50% of all values, i.e., the interquartile range (IQR,  $Q3-Q1$ ); the mean and median values are also shown. The whiskers represent the minimum and maximum values calculated as  $Q1 - 1.5 \times IQR$  and  $Q3 + 1.5 \times IQR$ , respectively. Data falling in the range between the lower and upper whiskers represent 99.3% of all the determined  $E^*$  values. The remaining 0.7% of the data points represent outliers with low statistical significance and are depicted with red diamond symbols outside of the whiskers. These cannot be completely avoided

during the measurement due to influences such as edge effects near the pores and particles; however, they have a negligible effect on the reported average values and trends.

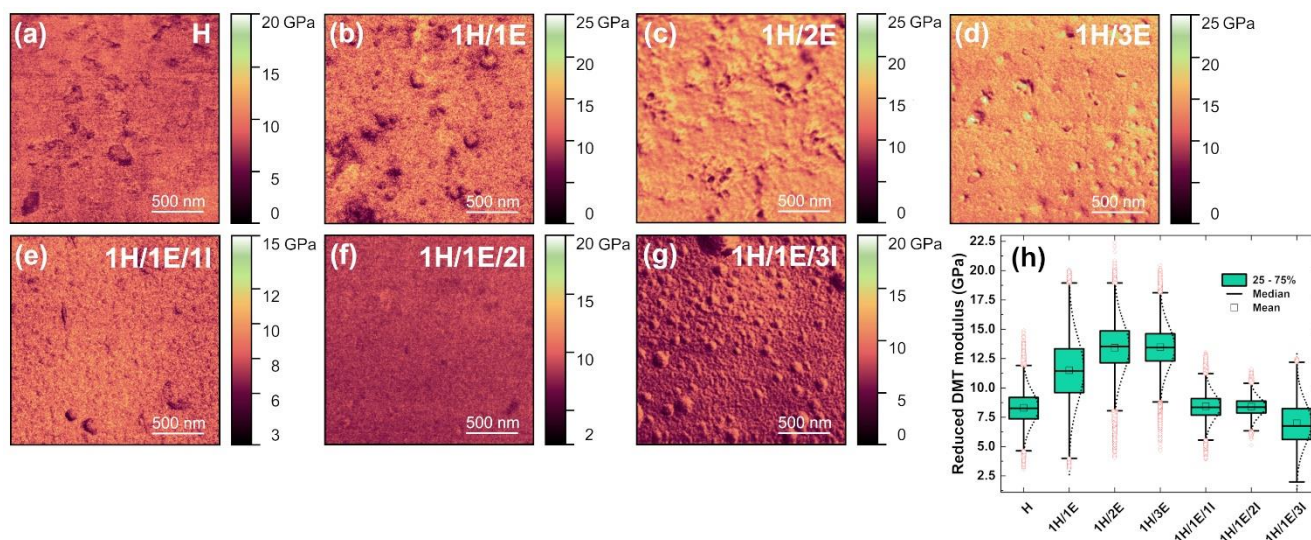


**Figure 9.** PF-QNM-determined reduced modulus maps showing the reduced elastic modulus for the (a) H, (b) 1H/1E, (c) 1H/2E, (d) 1H/3E, (e) 1H/1E/1I, (f) 1H/1E/2I, and (g) 1H/1E/3I films; (h) statistical distributions of reduced modulus for all films. The red diamond symbols represent the outliers corresponding to the 0.7% of the data points.

The  $E^*$  maps of investigated films were mostly homogeneous, but showed spatial variations which were typically correlated with the surface morphology, especially near the locations of the pores and particles (Figure 9). When probing such features, the probe's tip-to-sample area may vary significantly, which can be reflected in a lower accuracy of the determined values and artifacts, i.e., edge effects, and therefore, such results need to be treated cautiously.

As mentioned previously, one of the significant observed features in almost all samples was the existence of surface particles. Maps of the reduced modulus confirmed that these particles exhibited systematically lower values of  $\sim 6$ – $8$  GPa for all films, except for the 1H/1E/3I sample, in which their average modulus value was close to that of the whole scanned area. It is therefore likely that the surface particles observed in films H, 1H/1E, 1H/2E, 1H/3E, 1H/1E/1I, and 1H/1E/2I may have a similar origin, and their occurrence is closely related to the cross-linking process used. Also, since the particles were already present in the reference H film, it is likely that their occurrence in the cross-linked films may have originated from heparin, rather than from the cross-linkers used. The  $E^*$  map of the 1H/3E film in Figure 9d showed locations of higher-than-average values which are spatially correlated with the locations of the pores. We believe that rather than functioning as a true material property, these values represent unavoidable artefacts due to the varying contact area inside of the pores and close to their edges.

The following increasing order of the determined mean values of the surface reduced elastic modulus was found: 1H/1E/3I ( $\sim 7$  GPa) < H ( $\sim 8.2$  GPa) < 1H/1E/1I = 1H/1E/2I ( $\sim 8.4$  GPa) < 1H/1E ( $\sim 11.5$  GPa) < 1H/2E = 1H/3E ( $\sim 13.4$  GPa). A larger improvement of  $E^*$  was found for samples cross-linked with E; however, increased E content did not lead to a considerable increase in  $E^*$ . A similar increase was also observed for CCMC in comparison to CMC [18]. Compared to the reference H cross-linked 1H/1E, the 1H/2E and 1H/3E films showed approximately 40% and 63% higher  $E^*$  values. While increasing the E to H ratio to two led to an increase in the reduced modulus from 11.5 GPa to 13.4 GPa, no further significant increase was observed when higher E to H ratios were used, suggesting that the preparation conditions for the 1H/2E film were close to optimal. On the contrary, the films cross-linked with E in the presence of I showed negligible improvement of surface

$E^*$  (1H/1E/1I and 1H/1E/2I), or even its decrease by ~15% (1H/1E/3I). This seems to be due to the two limited nitrogen atoms on imidazole available for cross-linking. It is worth mentioning that despite the limited improvement of mechanical properties and the reduced modulus of substances in different ratios, the 1H/1E/1I and 1H/1E/2I films showed the narrowest spread between its values, reflecting improved surface morphology and a low number of particles. The 1H/1E/3I sample, displaying the largest roughness value, exhibits the smallest reduced modulus value.

#### 4. Conclusions

We prepared new heparin derivatives by cross-linking it with epichlorohydrin, in the absence (1H/1E, 1H/2E, 1H/3E) or presence of imidazole (1H/1E/1I, 1H/1E/2I, 1H/1E/3I), using substances in different ratios of H to E and I. According to the NMR results, the reaction took place on the end of the serine amino groups of the heparin motif: R-(1→4)- $\alpha$ -D-GlcNS6S-(1→4)- $\beta$ -D-GlcA-(1→4)- $\beta$ -D-Gal-(1→3)- $\beta$ -D-Gal-(1→3)- $\beta$ -D-Xyl- $\alpha$ -Ser. We assume that the observed decreased solubility of the 1H/1E/1I derivatives was caused by ionic interactions between the quaternary imidazolium groups and the uronic acid carboxyl, as measured by SEC-MALS analysis. We can further conclude that both types of derivatives exhibited higher molecular weights than that of the heparin substrate. The small increase in  $M_p$ , determined only on samples cross-linked with E, indicates that the main chain consisting of repeating H units was not modified by the cross-linking. According to the obtained yields, the highest value (77%) obtained for the 1H/1E sample resulted in the formation of the following derivative: H-(1→4)- $\beta$ -D-GlcA-(1→3)- $\beta$ -D-Gal-(1→3)- $\beta$ -D-Gal-(1→4)- $\beta$ -D-Xyl- $\alpha$ -Ser-CH<sub>2</sub>-CH(OH)-CH<sub>2</sub>-OH. The obtained sequence of yields, [1H/1E/3I (24%) < 1H/1E/2I (32%) < 1H/3E (42%) < 1H/1E/1I (46%) < 1H/2E (64%) < 1H/1E (77%)], indicates that imidazole was modified only monofunctionally, according to Figures 1 and 2. We assume that the formed positively charged imidazolium ring interacts with the negatively charged carboxyls of the serine carboxyl or uronic acids and the -SO<sub>3</sub><sup>-</sup> groups of H. This is related to the observed solubility of the samples: 1H/1E/1I (38.5%) < 1H/1E/3I (88.2%) < 1H/1E/2I (90.5%) < H (93.5%) < 1H/1E (98.1%) < 1H/2E (98.3%) < 1H/3E (99.0%). Considering the XRD and SEC-MALS results, we note that samples H, 1H/1E, 1H/2E, and 1H/3E, which showed the highest water-solubility, also showed the flattest diffractogram shape. The AFM-resolved surface roughness analysis of the prepared films revealed the following increasing order: 1H/2E (0.9 nm) < 1H/1E/2I (1.0 nm) < 1H/1E (2.1 nm) < 1H/1E/1I (2.2 nm) < 1H/3E (2.3 nm) < H (3.5 nm) < 1H/1E/3I (3.6 nm). The higher surface roughness was attributed to the presence of varying contents of pores and surface particles. On the other hand, only the 1H/1E/3I derivative displays a higher roughness than that of H. The reduced DMT surface elastic modulus of all the films was determined using the PF-QNM technique, and the following increasing order was found: 1H/1E/3I (~7 GPa) < H (~8.2 GPa) < 1H/1E/1I and 1H/1E/2I (~8.4 GPa) < 1H/1E (~11.5 GPa) < 1H/2E and 1H/3E (~13.4 GPa). The cross-linked films prepared without the presence of I showed improved values of the reduced modulus, i.e., up to ~63% for the 1H/2E and 1H/3E films. In contrast, the films cross-linked in the presence of I showed negligible improvement (1H/1E/1I and 1H/1E/2I), or even a ~15% decrease (1H/1E/3I) in the surface elastic modulus. However, the  $E^*$  values of the two former films exhibited the narrowest spread of all studied samples, reflecting an improved surface morphology and a low number of particles. The described process can be useful for various applications in medical instrumentation, e.g., to form film composites on plastic surfaces for kidney dialysis equipment [13] and for the treatment of pulmonary embolism or problems related to thrombus dissolution [14].

**Author Contributions:** Conceptualization: I.Š., F.G. and M.H. (Miloš Hricovíni); formal analysis: M.H. (Michal Hricovíni), F.G. and E.D.; funding acquisition: M.H. (Miloš Hricovíni); investigation: I.Š., F.G., M.H. (Michal Hricovíni), R.M. and E.D.; methodology: I.Š., F.G., M.H. (Miloš Hricovíni) and R.M.; project administration: I.Š. and M.H. (Miloš Hricovíni); supervision: I.Š.; validation: I.Š., F.G., R.M. and M.H. (Miloš Hricovíni); visualization: I.Š. and F.G.; writing—original draft: I.Š.;

writing—review and editing: I.Š., F.G., M.H. (Michal Hricovíni), M.H. (Miloš Hricovíni), R.M., E.D., A.G.S., D.P. and S.Z. All authors have read and agreed to the published version of the manuscript.

**Funding:** M.H. (Miloš Hricovíni) is grateful for a supporting grant provided by the Slovak Grant Agency VEGA (Project #2/0071/22).

**Institutional Review Board Statement:** This research did not involve human or animal samples.

**Data Availability Statement:** Data are contained within the article, further request please contact the corresponding author.

**Conflicts of Interest:** The authors declare no conflicts of interest.

## References

1. Liu, L.; Huan, Y.; Wang, L.; Zhao, D.; Duan, X.; Zhang, X.; Yin, J.; Luan, S.; Shi, H. Heparin-network-mediated long-lasting coatings on intravascular catheters for adaptive antithrombosis and antibacterial infection. *Nat. Commun.* **2024**, *15*, 107. [[CrossRef](#)] [[PubMed](#)]
2. Šimkovic, I. Unexplored possibilities of all-polysaccharide composites. *Carbohydr. Polym.* **2013**, *95*, 697–715. [[CrossRef](#)] [[PubMed](#)]
3. Malsch, R.; Guerrini, M.; Torri, G.; Löhr, G.; Casu, B.; Harenberg, J. Synthesis of N'-alkylamine anticoagulant active low-molecular-mass heparin for radioactive and fluorescent labelling. *Anal. Biochem.* **1994**, *217*, 255–267. [[CrossRef](#)]
4. Šimkovic, I.; Mendichi, R.; Kelnar, I.; Filip, J.; Hricovíni, M. Cationization of heparin for film applications. *Carbohydr. Polym.* **2015**, *115*, 551–558. [[CrossRef](#)]
5. Muir, V.G.; Burdik, J.A. Chemically modified biopolymers for the formation of biomedical hydrogels. *Chem. Rev.* **2021**, *121*, 10908–10949. [[CrossRef](#)] [[PubMed](#)]
6. Šimkovic, I.; Laszlo, J.A. Preparation of ion exchangers from bagasse by crosslinking with epichlorohydrin-NH<sub>4</sub>OH or epichlorohydrin-imidazole. *J. Appl. Polym. Sci.* **1997**, *64*, 2561–2566.
7. Šimkovic, I.; Hricovíni, M.; Šoltés, L.; Mendichi, R. Preparation of water-soluble/insoluble derivatives of hyaluronic acid by cross-linking with epichlorohydrin in aqueous NaOH/NH<sub>4</sub>OH solution. *Carbohydr. Polym.* **2000**, *41*, 9–14. [[CrossRef](#)]
8. Šimkovic, I.; Mlynár, J.; Alföldi, J.; Micko, M.M. New aspects in cationization of lignocellulose materials. XI. Modification of bagasse with quaternary ammonium groups. *Holzforschung* **1990**, *44*, 113–116. [[CrossRef](#)]
9. Šimkovic, I.; Mlynár, J.; Alföldi, J. Modification of corn cob meal with quaternary ammonium groups. *Carbohydr. Polym.* **1992**, *17*, 285–288. [[CrossRef](#)]
10. Mauri, L.; Boocardi, G.; Torri, G.; Karfunkle, M.; Macchi, E.; Muzi, L.; Kaire, M. Qualification of HSQC methods for quantitative composition of heparin and low molecular weight heparins. *J. Pharm. Biomed. Anal.* **2017**, *136*, 92–105. [[CrossRef](#)]
11. Perez, S.; Makshakova, O.; Angulo, J.; Bedini, E.; Bisio, A.; de Paz, J.L.; Fadda, E.; Guerrini, M.; Hricovíni, M.; Hricovíni, M.; et al. Glycosaminoglycans: What remains to be deciphered? *J. Amer. Chem. Soc. Au* **2023**, *3*, 628–656. [[CrossRef](#)] [[PubMed](#)]
12. Su, L.; Feng, Y.; Wei, K.; Xu, X.; Liu, R.; Chen, G. Carbohydrate-based macromolecular biomaterials. *Chem. Rev.* **2021**, *121*, 10950–11029. [[CrossRef](#)] [[PubMed](#)]
13. Murugesan, S.; Mousa, S.; Vijayaraghavan, A.; Ajayan, P.M.; Linhardt, R.J. Ion liquid-derived blood-compatible composite membranes for kidney dialysis. *J. Biomed. Mater. Res. B Appl. Biomater.* **2006**, *79B*, 298–304. [[CrossRef](#)] [[PubMed](#)]
14. Kozłowski, J.A.; Dinu, V.; MacCalman, T.; Smith, A.M.; Roubroeks, J.P.; Yates, E.A.; Harding, S.E.; Morris, G.A. Heparin in acid and Alkaline environments – a study of the correlations between hydrodynamic properties and desulphation. *Polysaccharides* **2023**, *4*, 349–355.
15. Nosov, D.R.; Loyinskaya, E.I.; Antonov, D.Y.; Ponkratov, D.O.; Tyutyunov, A.A.; Eddine, M.A.; Plesse, C.; Schmidt, D.F.; Shaplov, A.S. Design of highly conductive PILs by simple modification of poly(epichlorohydrin-co-ethylene oxide) with monosubstituted imidazole. *ACS Polym. Au* **2024**. [[CrossRef](#)]
16. Nguyen, K.; Rabenstein, D.L. Determination of the primary structure and carboxyl pK<sub>As</sub> of heparin-derived oligosaccharides by band-selective homonuclear-decoupled two-dimensional <sup>1</sup>H NMR. *Analytical. Bioanal. Chem.* **2011**, *399*, 663–671. [[CrossRef](#)]
17. Šimkovic, I.; Gucmann, F.; Hricovíni, M.; Mendichi, R.; Giacometti Schieroni, A.; Piovani, D.; Zappia, S.; Dobročka, E.; Filip, J.; Hricovíni, M. Properties of quaternized and crosslinked carboxymethylcellulose films. *Cellulose* **2023**, *30*, 2023–2036. [[CrossRef](#)]
18. Sader, J.E.; Sanelli, J.A.; Adamson, B.D.; Monty, J.P.; Wei, X.; Crawford, S.A.; Friend, J.R.; Marusic, I.; Mulvaney, P.; Bieske, E.J. Calibration of rectangular atomic force microscope cantilevers. *Rev. Sci. Instrum.* **2012**, *83*, 103705. [[CrossRef](#)]
19. Butt, H.J.; Cappella, B.; Kappl, M. Force measurements with the atomic force microscope: Technique, interpretation and applications. *Surf. Sci. Rep.* **2005**, *59*, 1–152.
20. Muller, V.M.; Derjaguin, B.V.; Toporov, Y.P. On two methods of calculation of the force of sticking of an elastic sphere to a rigid plane. *Colloids. Surf.* **1983**, *7*, 251–259. [[CrossRef](#)]
21. Keire, D.A.; Buhse, L.F.; al-Hakim, A. Characterization of currently marketed heparin products: Composition analysis by 2D-NMR. *Anal. Meth.* **2015**, *5*, 2984–2994. [[CrossRef](#)]
22. Jogala, S.; Rachamalla, S.S.; Aukunuru, J. Development of subcutaneous sustained release nanoparticles encapsulating low molecular weight heparin. *J. Adv. Pharm. Technol. Res.* **2015**, *6*, 58–64. [[PubMed](#)]

23. Maurier, P.; Anger, P.; Martinez, C.; Herman, F.; Viskov, C. Quantitative compositional analysis of heparin using exhaustive heparinase digestion and strong anion exchange chromatography. *Anal. Chem. Res.* **2015**, *3*, 46–53. [[CrossRef](#)]
24. Meng, N.; Zhou, N.L. Synthesis and properties of PDMS/montmorillonite-cetyltrimethylammonium bromide-heparin films. *Carbohydr. Polym.* **2014**, *105*, 70–74. [[CrossRef](#)]
25. Urbaniak, T.; Garcia-Briones, G.S.; Zhigunov, A.; Hladysz, S.; Adrian, E.; Lobaz, V.T.; Krunclová, T.; Janoušková, O.; Pop-Gegorgievski, O.; Kubies, D. Quaternized Chitosan/Heparin polyelectrolyte multilayer films for protein delivery. *Biomacromolecules* **2022**, *23*, 4734–4748. [[CrossRef](#)]
26. Šimkovic, I.; Gucmann, F.; Mendichi, R.; Giacometti Schieroni, A.; Piovani, D.; Dobročka, E.; Hricovíni, M. Extraction and characterization of polysaccharide films from *Furcellaria lumbricalis* and *Gigartina skottsbergii* seaweeds. *Cellulose* **2021**, *28*, 9567–9588. [[CrossRef](#)]

**Disclaimer/Publisher’s Note:** The statements, opinions and data contained in all publications are solely those of the individual author(s) and contributor(s) and not of MDPI and/or the editor(s). MDPI and/or the editor(s) disclaim responsibility for any injury to people or property resulting from any ideas, methods, instructions or products referred to in the content.